MULTIGRID SCHEMES FOR VISCOUS HYPERSONIC FLOWS

$S9-02$

197569

$P- 15$

R. Radespiel
DLR, Braunschweig
Germany

R. C. Swanson
NASA Langley Research Center
Hampton, VA 23681

ABSTRACT

Several multigrid schemes are considered for the numerical computation of viscous hypersonic flows. For each scheme, the basic solution algorithm employs upwind spatial discretization with explicit multistage time stepping. Two-level versions of the various multigrid algorithms are applied to the two-dimensional advection equation, and Fourier analysis is used to determine their damping properties. The capabilities of the multigrid methods are assessed by solving two different hypersonic flow problems. Some new multigrid schemes, based on semicoarsening strategies, are shown to be quite effective in relieving the stiffness caused by the high-aspect-ratio cells required to resolve high Reynolds number flows. These schemes exhibit good convergence rates for Reynolds numbers up to 200×10^6.

INTRODUCTION

In the past several years, multigrid has been used to accelerate the convergence of Navier-Stokes computations for a variety of flow problems at both subsonic and transonic speeds (refs. 1 and 2). More recently, multigrid methods with either central or upwind differencing have been applied to viscous hypersonic flows to achieve convergence rates that approach those obtained at lower Mach numbers and moderate Reynolds numbers ($Re < 10^7$). However, at the higher Re values experienced by high-speed flight vehicles, a dramatic slowdown occurs in the convergence rate. One reason for this slowdown is the deterioration in the high-frequency damping of the multigrid driving scheme caused by the very high-aspect-ratio cells that occur in the computational mesh in order to resolve the thin boundary layers.

The present paper describes an effort to understand and improve the use of multigrid schemes for the computation of viscous hypersonic flows. First, various two-level multigrid schemes both with and without semicoarsening are introduced. Then we use a Fourier analysis of the schemes, applied to the two-dimensional convection equation, to reveal the behavior of their components. For each multigrid approach, the solver uses an upwind discretization combined with an explicit multistage scheme. We next consider the numerical solution of the Navier-Stokes equations for hypersonic flows. The basic elements of the flow solver for these equations are summarized. Some details concerning the application of

the time-stepping scheme to fine- and coarse-grid problems are presented. The extension of the two-level schemes to multilevel ones is then discussed. Elements of multigrid that are of particular importance for high-speed flow computations are given. In the results section, we consider two different hypersonic flow problems to assess the capabilities of the multigrid schemes. Semicoarsening is shown to be quite effective in relaxing the stiffness that arises from the resolution of thin boundary layers.

MULTIGRID METHOD AND STRATEGIES

The multigrid approach is based on the full approximation scheme of Brandt (ref. 3). The grid transfer operators are those considered by Jameson (ref. 4). Coarser meshes are obtained by eliminating alternate mesh points in each coordinate direction. Both the solution and the residuals are restricted from fine to coarse meshes. A forcing function is constructed so that the solution on a coarse mesh is driven by the residuals collected on the next finer mesh. The corrections obtained on the coarse mesh are interpolated back to the fine mesh. The multigrid schemes investigated within the present work are displayed in Figure 1. Figure 1(a) shows a two-level scheme with full coarsening. Restriction of the solution from the fine mesh (m,n) to the coarse mesh (m/2,n/2) is done by injection, whereas full weighting is used for the restriction of the residuals. Prolongation of the corrections is done by bilinear interpolation. Figure 1(b) shows a scheme with semicoarsening in the different coordinate directions. Again, injection and full weighting are used in the restriction process. The corrections obtained on the coarse meshes are averaged before they are added to the current fine mesh solution which is indicated by the numbers at the "up" arrows. Because of this averaging, half of the individual corrections on the coarse meshes are lost. We, therefore, anticipate that the scheme in Figure 1(a) should be computationally more efficient, provided that enough high-frequency damping can be obtained with the smoothing scheme of the fine mesh. In order to overcome this deficiency of the semicoarsening scheme, two more variants are considered. For the scheme of Figure 1(c), the solutions on the coarse meshes are computed sequentially. Hence, the corrections obtained on the (m/2,n) mesh can be used to update the (m,n/2) mesh before time stepping (as indicated by the horizontal arrow). The sequential update of the second coarse mesh allows the full corrections to be passed up to the fine mesh. Note that this multigrid variant is not compatible with the idea of parallel computations. An interesting compromise between the schemes of Figures 1(b) and 1(c) was suggested by Van Rosendale based on the work of ref. 5 (Figure 1(d)). Here, only the corrections common to both of the coarse meshes, (m/2,n) and (m,n/2), are averaged, whereas the corrections to the modes that live either on (m/2,n) or on (m,n/2) are passed to the fine mesh in full. This scheme does allow parallel computations for the coarse meshes.

FOURIER ANALYSIS OF THE SCALAR ADVECTION EQUATION

A crucial factor in constructing an effective multigrid method is the selection of a smoothing or driving scheme. Local mode (Fourier) analysis is generally applied to evaluate possible smoothers on the basis of stability and high-frequency damping properties. The

screening of schemes is often performed with a single-grid analysis. Since a stable single-grid scheme may not be stable for the multigrid process, the behavior of a smoother with a particular multigrid strategy is needed. In addition, the multigrid process can have a substantial impact on the performance of the multigrid method. In fact, as we will demonstrate in this paper, semicoarsening can provide significant improvement, relative to full coarsening, in the damping of the multigrid, especially when a strong mesh anisotropy is present due to the high-aspect-ratio cells.

In ref. 4, Jameson models a multigrid scheme as a multilevel uniform scheme and analyzes the stability of this scheme when applied to the linear advection equation in one space dimension. With the multilevel uniform scheme, fine-grid and coarse-grid corrections are computed at all points of the fine grid. Then, a nonlinear filter is applied to remove the coarse-grid corrections at fine-grid points not contained in the coarse grid. The filtering produces additional errors in the form of a carrier wave with a frequency depending on the fine-mesh spacing. This approach does not allow for the coupling (aliasing) effects due to the restriction operator (fine to coarse grid transfer operator) in the multigrid method. However, it does offer the advantages of simplicity and application to more than two-level schemes. Thus, it allows the rapid comparison of multigrid algorithms. If a multigrid method is unstable or inefficient according to Fourier analysis of the multilevel uniform scheme, then it is probably not a reasonable scheme.

In ref. 6 we consider the scalar two-dimensional advection equation and perform a Fourier analysis of the multilevel uniform scheme for different multigrid strategies. The effects of mesh-cell aspect ratio are included in the analysis. For details of the analysis, see ref. 6. Here, as in ref. 6, a five-stage scheme with three weighted evaluations of the numerical dissipation is used for a solver. The explicit stability limit of this scheme is extended with variable-coefficient implicit residual smoothing, which results in a Courant-Friedrichs-Lewy (CFL) number of 5. A two-level analysis is applied to both full coarsening and semicoarsening strategies. Figure 2 presents contours of the amplification factor g as a function of Fourier phase angles for the full coarsening and sequential semicoarsening strategies when the mesh-cell aspect ratio (AR) was set to 10. Even with this AR, one can clearly see the improved damping (reduced g) in the direction of the long side of the cell with sequential semicoarsening.

SPATIAL DISCRETIZATION

A finite-volume approach, where the flow quantities are stored at the cell vertices, is used for the spatial discretization of the Navier-Stokes equations. For the convective flux calculation, an auxiliary grid is used, which is defined by connecting the cell centers of the original cells (see Figure 3). The inviscid numerical flux is separated into the sum of an averaged term that corresponds to central differencing and a dissipative term that adapts the discretization stencil in accordance with local wave propagation. The dissipative flux function is based on the second-order-accurate upwind scheme of Yee and Harten (ref. 7). In the case of viscous flows the entropy correction for this scheme must be carefully designed, as discussed in ref. 6. The physical viscous fluxes are approximated by central differences with a local transformation from Cartesian to curvilinear coordinates (ref. 2).

MULTISTAGE SCHEME FOR THE FINE AND COARSE MESHES

We have observed the need to pair spatial discretization and particular time-stepping schemes for the solution of the Navier-Stokes equation. The most robust choice of spatial discretizations found to this point is to use a second-order upwind scheme on the fine meshes and to set the limiter to zero everywhere on the coarse meshes. An alternative taken in refs. 8 and 9 is to use scalar second-difference dissipation terms on the coarse meshes. This approach turned out to be less robust because the second differences are less diffusive with respect to the acoustic modes; also, the central-difference scheme allows waves to travel upstream in supersonic flow. As indicated previously, a five-stage explicit scheme with three evaluations of dissipation is used for time advancement. Disturbances are most effectively expelled out of the computational domain by using local time stepping and implicit residual smoothing (refs. 8 and 10). The smoothing of the residuals allows the CFL number of the explicit scheme to be as high as 5.75, which extends the stability limit (CFL*) by a factor of 2.5. The time step is proportional to the ratio of the cell volume to the sum of the spectral radii of the inviscid flux Jacobians in the different coordinate directions.

To stabilize the schemes in regions where the viscous stability limit is more restrictive than the inviscid limit, the coefficients of the implicit residual smoothing operator are locally increased, as outlined in refs. 8 and 9. At strong shocks, however, high Courant numbers are not appropriate. Consequently, an adaptive time step is employed. By using the nondimensional second difference of the pressure as a switch, the value of CFL is locally reduced to approximately 2 at the shock.

MULTIGRID SCHEMES

For the numerical solution of the Navier-Stokes equations, the two-level strategies presented in Figure 1 are extended to multilevel schemes, as displayed in Figure 4. The only differences between the two-level schemes and the multilevel schemes occur in the restriction process. Whenever two "down" arrows meet at a coarse mesh, averaging is used to obtain the restricted variable. The multilevel arrangement of the coarse meshes, shown in Figure 4(b), was first given by Mulder (ref. 11), who used semicoarsening to solve the flow alignment problem. Suitable coordinate meshes for thin boundary layers exhibit mostly cells with high aspect ratios in the surface-aligned direction. In this paper, other variants of semicoarsening, which are computationally cheaper than the semicoarsening schemes shown in Figure 4, are also considered for these situations.

One may notice that the central restriction and prolongation operators discussed previously allow for upstream propagation of disturbances in supersonic flow. Furthermore, the corrections given by the standard multigrid scheme near strong shocks lead to divergence of the calculation, especially when free-stream initial conditions are used. Therefore, the restriction operator is damped by using

$$R_{i,j} = \max\left(1 - \epsilon_{i,j}^{(n)}, 0\right)\bar{R}_{i,j}, \tag{1}$$

where $\bar{R}_{i,j}$ is the standard restriction operator and $\epsilon_{i,j}^{(n)}$ is a switch to detect strong

shocks, and

$$\epsilon_{i,j}^{(n)} = k^{(n)} \max \left(\nu_i, \nu_{i+1}, \nu_{i-1}, \nu_j, \nu_{j+1}, \nu_{j-1}\right), \tag{2}$$

$$\nu_i = \left|\frac{p_{i-1,j} - 2p_{i,j} + p_{i+1,j}}{p_{i-1,j} + 2p_{i,j} + p_{i+1,j}}\right|, \qquad \nu_j = \left|\frac{p_{i,j-1} - 2p_{i,j} + p_{i,j+1}}{p_{i,j-1} + 2p_{i,j} + p_{i,j+1}}\right|, \tag{3}$$

where p denotes pressure. The damping coefficient $k^{(n)}$ is given a value of approximately 1 in the start-up phase of the multigrid process and is decreased to a value of about 0.4 at later cycle numbers to allow for good asymptotic convergence rates. Such a local damping with a $k^{(n)}$ that does not vanish is in line with the restriction damping of Koren and Hemker (ref. 12), who based their damping coefficients on a more physical analysis.

A fixed V-type cycle with time stepping only on the way down is used to execute the multigrid strategies described above. The robustness of the overall scheme is improved by smoothing the resultant coarse-mesh corrections before they are passed to the finest mesh. The smoothing reduces the high-frequency oscillations introduced by the linear interpolation of the coarse-mesh corrections. The implicit residual smoothing procedure with constant coefficients of around 0.1 is used for this smoothing. Also, the application of full multigrid (FMG) provides a well-conditioned starting solution for the finest mesh that is considered.

NUMERICAL RESULTS

Two different hypersonic flow cases are used to assess the capabilities of the multigrid schemes. These are laminar Mach 10 ($M = 10$) flow over a compression ramp and turbulent flow over a slender forebody at high Reynolds numbers. Table 1 gives a summary of the geometries and the flow parameters of the test cases. In this table, T_{inf} is the dimensional free-stream temperature, and T_w is the specified wall temperature. Also, the finest grid used for each flow computation is characterized by the streamwise and normal leading-edge spacings Δs_{le}, Δn_{le}, with the normal spacing Δn_{te} at the end of the geometry.

The flow over the compression ramp is identical to case 3.2 of the Workshop on Hypersonic Flows for Reentry Problems, Part II, held in Antibes, France, in 1991. This allows comparisons with the performance of other computational methods published in ref. 13. Figure 5 displays the coordinate mesh generated for this test case. The low Reynolds number allows for a mesh with moderate aspect ratios between 5 and 50 near the wall. The 129 × 81 mesh is successively coarsened down to 9 × 6, which yields 9 grid levels with semicoarsening and 5 levels with full coarsening. The semicoarsening strategy is expected to eliminate most of the stiffness associated with aspect ratio. The converged flow solution is shown in Figure 6 for the 129 × 81 and 65 × 41 grids. The computed extent of separation in the corner is somewhat smaller for the coarse mesh than for the fine mesh. The fine-mesh results agree well with grid-converged computations published in ref. 14.

In the next figures, we investigate the performance of the different multigrid schemes. For this purpose, computations were started from a solution that was converged to about plotting accuracy. Results from the different schemes of Figure 4 are compared in Figure 7. The numbers indicate the final convergence rate r of the schemes and the rate of data processing (RDP) on a CRAY-YMP to advance one grid point by one multigrid cycle.

The sequential semicoarsening scheme (Figure 4(c)) gives by far the best convergence rate. For this scheme, the effect of the modifications in the multigrid strategies of Figure 4 is investigated in Figure 8. The meshes obtained by full coarsening and by semicoarsening in the direction normal to the wall are both important in achieving good convergence rates. From Figures 7 and 8, we conclude that semicoarsening with a selected number of coarse meshes is most effective for this flow problem. Semicoarsening is about 2.4 times faster than full coarsening, which does a surprisingly good job because of its low work count. In particular, the multigrid scheme with sequential semicoarsening converges (i.e., the residual was reduced 3 orders of magnitude) in roughly 33 sec (CPU time) on a Cray-YMP, which is 10 times faster than the single-mesh scheme.

The flow over a slender forebody is chosen to represent a generic configuration that corresponds to a high-speed civil transport aircraft or an air-breathing space transportation system with low wave drag. The high Reynolds numbers yield thin boundary layers, which can only be resolved with highly clustered coordinate meshes and large-aspect-ratio cells. The mesh used for the present investigations is displayed in Figure 9. The cells near the wall have aspect ratios up to 25000. The flow computations were done with fixed transition at 2 percent chord and with the assumption of an adiabatic wall. Figure 10 shows the Mach contours for the mesh of 256×96 cells, and Figures 11 and 12 show the solution obtained on three successively refined meshes. Both the distributions of the skin friction and the wall temperature are accurately computed, even with only 25 points in the normal direction.

Next we examine the convergence behavior of the multigrid schemes. The fine mesh with 257×97 points allows 11 grid levels to be used with semicoarsening. The full diamond-shaped tree of coarse meshes cannot be run because the time-stepping scheme is not well suited to handle the extreme aspect ratios that occur on the coarse meshes. With the proper half of the diamond, which includes the meshes with relatively low aspect ratios, the numerical solution converges. Figure 13 displays a comparison of the different multigrid strategies. The computations are started from a preconverged solution. Again, the scheme with sequential semicoarsening converges best. The differences between the multigrid schemes for this case, which has cells with very high aspect ratios, are larger than for the ramp flow. The final convergence rate of the scheme with sequential semicoarsening is 15 times better than the rate with full coarsening. A comparison of the performance for the complete FMG process is given in Figure 14. The sequential semicoarsening scheme takes 194 cycles and 570 sec to reduce the averaged residuals to 10^{-2} on the fine mesh. The scheme with full coarsening takes 1024 cycles and 1430 sec, and the single mesh code takes 7762 time steps and 6190 sec to achieve the same convergence level. Note that residuals of 10^{-2} correspond to a solution that is converged within plotting accuracy. If we compared computer times to reach lower levels of residuals instead, then the results would have been even better for the multigrid scheme with semicoarsening.
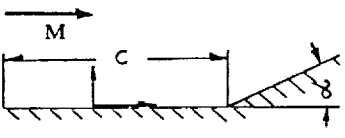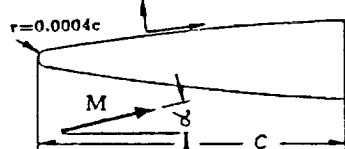
CONCLUSIONS

New multigrid schemes for hypersonic flow computations have been investigated. The basic solution algorithm employs upwind discretization and explicit multistage time stepping. Various multigrid schemes with semicoarsening are introduced to overcome the

stiffness that results from the high-aspect-ratio mesh cells used to resolve viscous flows. The basic components of the algorithm are examined with a Fourier stability analysis applied to the two-dimensional advection equation. Both the results of the Fourier analysis and the computations of high Reynolds number flows suggest that the semicoarsening approach is effective. The convergence rates shown for hypersonic viscous flows are similar or even better than those previously published for the transonic regime in refs. 1 and 2. Further work is required to make the computational scheme less expensive. This need for more research is particularly true for the coarse meshes used within the semicoarsening approach, which make up the major portion of the overall work count of the scheme.

REFERENCES

1. Radespiel, R.; Rossow, C.; and Swanson, R. C.: An Efficient Cell-Vertex Multigrid Scheme for the Three-Dimensional Navier-Stokes Equations. *AIAA J.*, vol. 28, no. 8, 1990, pp. 1464-1472.
2. Swanson, R. C.; and Radespiel, R.: Cell Centered and Cell Vertex Multigrid Schemes for the Navier-Stokes Equations. *AIAA J.*, vol. 29, no. 5, 1991, pp. 697-703.
3. Brandt, A.: Multi-Level Adaptive Solutions to Boundary-Value Problems. *Math. Comp.*, vol. 31, no. 138, 1977, pp. 333-390.
4. Jameson, A.: Multigrid Algorithms for Compressible Flow Calculations. *Lecture Notes in Mathematics*, vol. 1228, Springer-Verlag, 1986, pp. 166-201.
5. Naik, N. H.; and Van Rosendale, J.: The Improved Robustness of Multigrid Elliptic Solvers Based on Multiple Semicoarsened Grids. *SIAM J. Numer. Anal.*, vol. 30, no. 1, 1993, pp. 215-229.
6. Radespiel, R.; and Swanson, R. C.: Progress with Multigrid Schemes for Hypersonic Flow Problems. NASA CR-189579, Dec. 1991.
7. Yee, H. C.; and Harten, A.: Implicit TVD Schemes for Hyperbolic Conservation Laws in Curvilinear Coordinates. *AIAA J.*, vol. 25, 1987, pp. 266-274.
8. Turkel, E.; Swanson, R. C.; Vatsa, V. N.; and White, J. A.: Multigrid for Hypersonic Viscous Two- and Three-dimensional Flows. AIAA Paper 91-1572-CP, 1991.
9. Radespiel, R.; and Kroll, N.: Multigrid Schemes with Semicoarsening for Accurate Computations of Hypersonic Viscous Flows. Tagungsband 7, DGLR-Fachsymposium "Strömungen mit Ablösung", Aachen, Nov. 7-9, 1990, DGLR-Bericht 91-5, 1990.
10. Swanson, R. C.; Turkel, E.; and White, J. A.: An Effective Multigrid Method for High-Speed Flows. *Commun. Appl. Numer. Methods*, vol. 8, no. 9, 1992, pp. 671-681.
11. Mulder, W. A.: A New Multigrid Approach to Convection Problems. *J. of Comput. Phys.*, vol. 83, 1989, pp. 303-323.
12. Koren, B.; and Hemker, P. W.: Damped, Direction-Dependent Multigrid for Hypersonic Flow Computations. *Appl. Numer. Math.*, vol. 7, 1991, pp. 309-328.
13. Abgrall, R. et al., ed.: *Hypersonic Flows for Reentry Problems*, vol. 3. Springer-Verlag, 1992.
14. Thomas, J. L.: An Implicit Multigrid Scheme for Hypersonic Strong-Interaction Flowfields. *Commun. Appl. Numer. Methods*, vol. 8, no. 9, 1992, pp. 683-693.

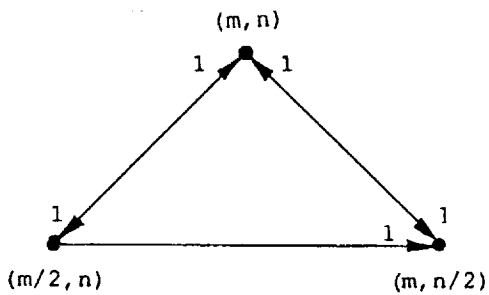# Table 1. Flow and geometric parameters for test cases

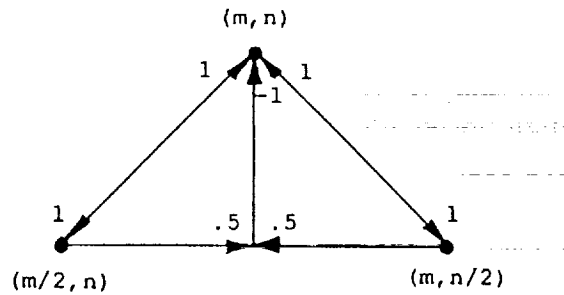| Flow Case	M	α	Re_c	T_{inf}	T_w/T_{inf}	$No.Pts.$	$\Delta s_{le}/c$	$\Delta n_{le}/c$	$\Delta n_{te}/c$
	10	20°	18119	52K	5.57	129x81	0.004	0.0008	0.0008
	7	5°	2.E8	100K	adiab.	257x97	4.4E-5	2.E-7	2.E-6
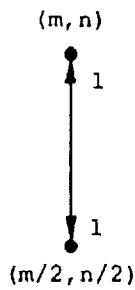
(a) Full coarsening.
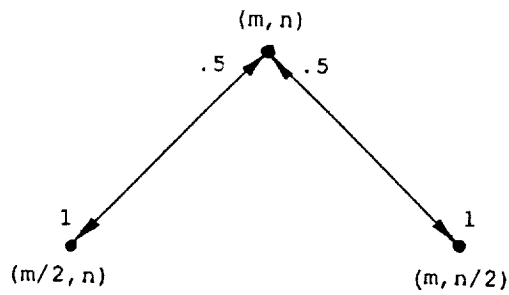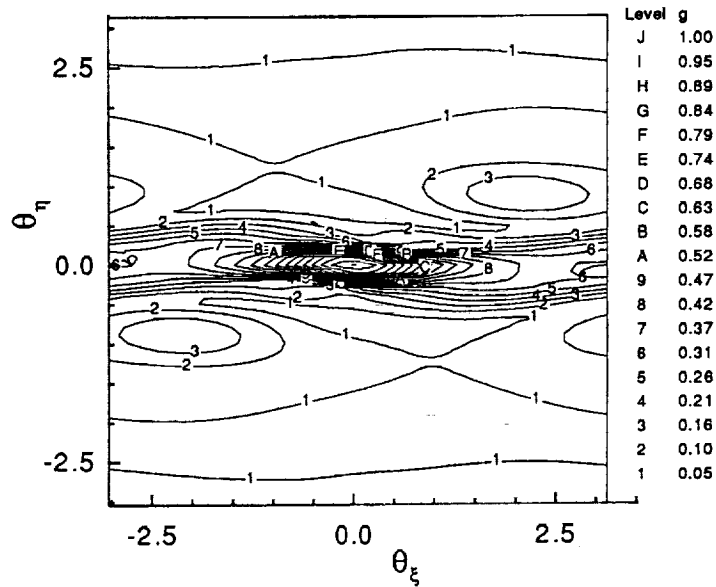
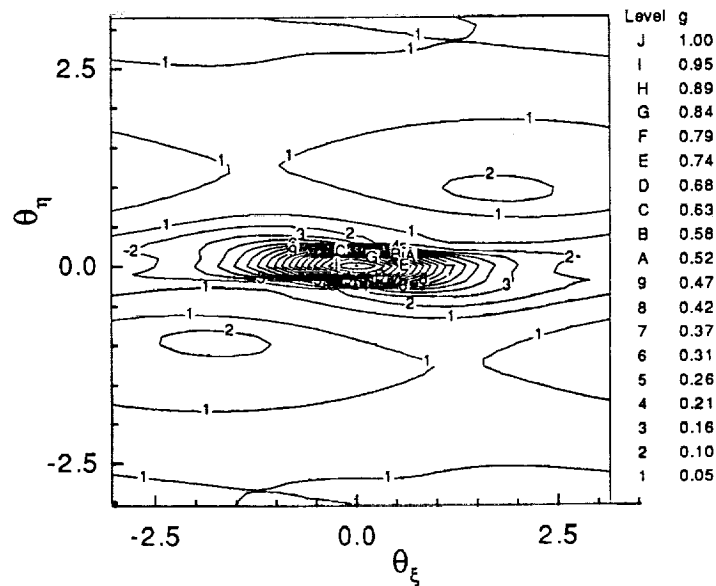(b) Semicoarsening with simple averaging.

(c) Sequential semicoarsening.

(d) Semicoarsening with selective averaging.

Figure 1. Two-level multigrid schemes investigated in present work.

(a) Two levels, full coarsening, AR = 10 (CFL = 5.0, CFL* = 2.4).

(b) Two levels, sequential semicoarsening, weights = 1.0, AR = 10 (CFL = 5.0, CFL* = 2.4).

Figure 2. Contour plots of amplification factor for 5-stage Runge-Kutta
scheme with first-order upwind approximation and 3 evaluations
of dissipation (coefficients : 0.2742, 0.2067, 0.5020, 0.5142, 1.0).
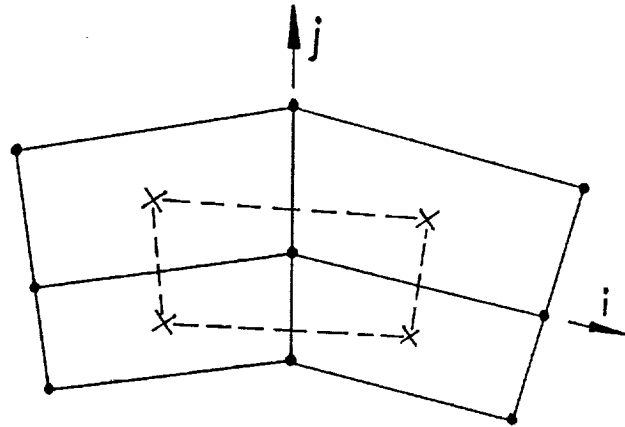
Figure 3. Control volume for nodal-point scheme.

(a) Full coarsening.
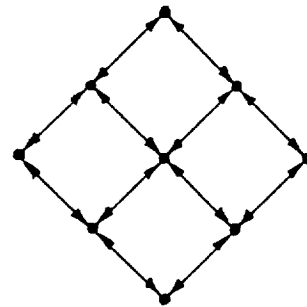
(b) Semicoarsening with simple averaging.
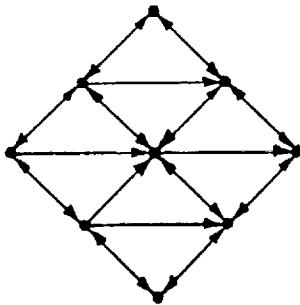
(c) Sequential semicoarsening.
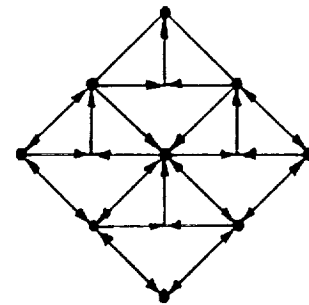
(d) Semicoarsening with selective averaging.

Figure 4. Multilevel schemes.
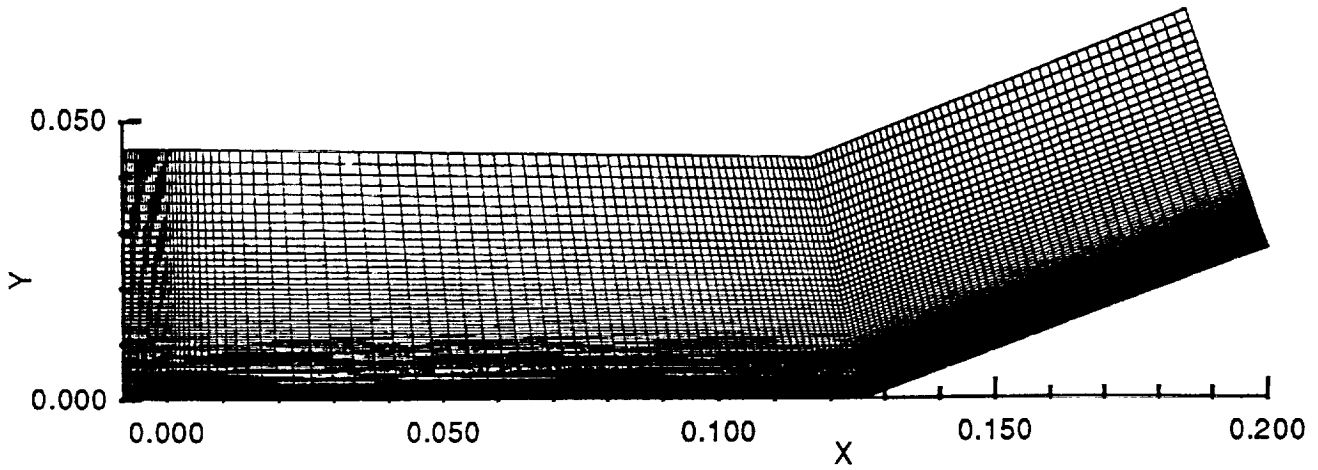
Figure 5. Coordinate mesh for ramp-flow problem with 128x80 cells.
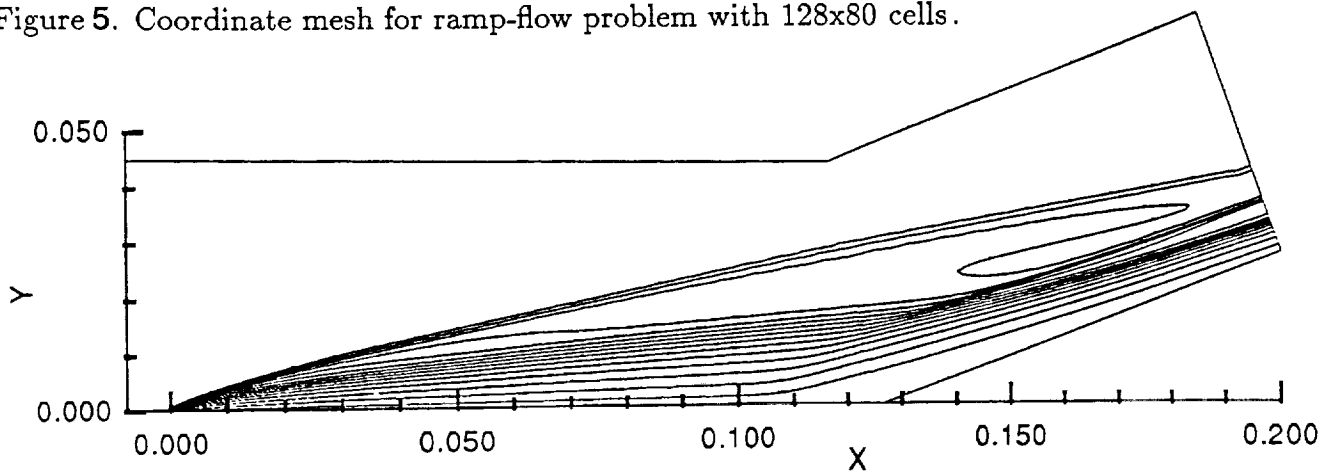
(a) Mach contours.
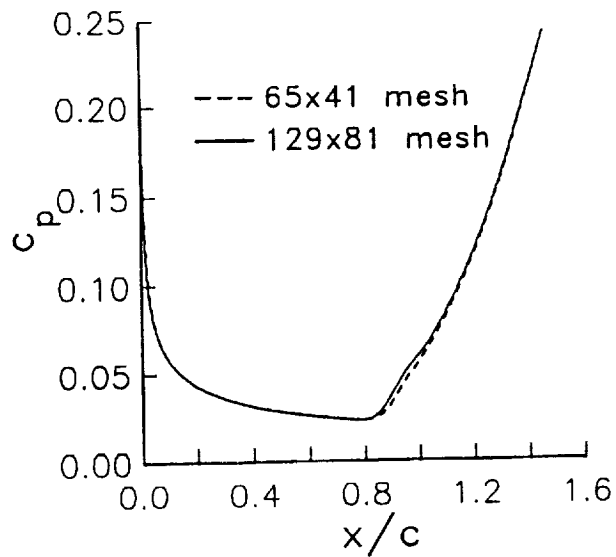
(b) Pressure coefficient.
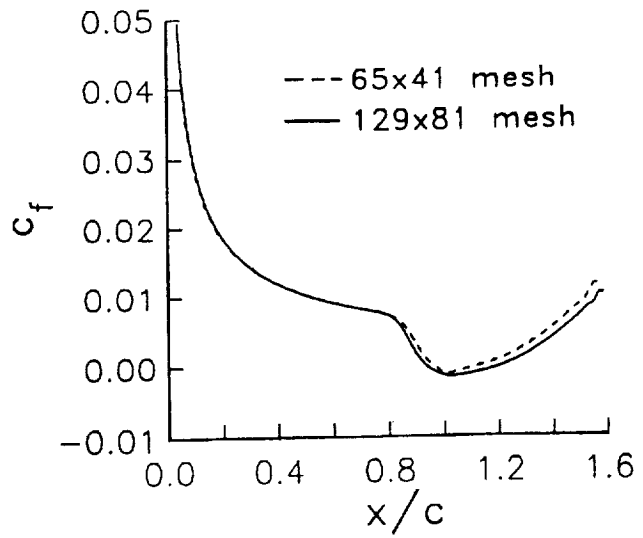
(c) Skin friction.

Figure 6. Flow solution for ramp-flow problem.
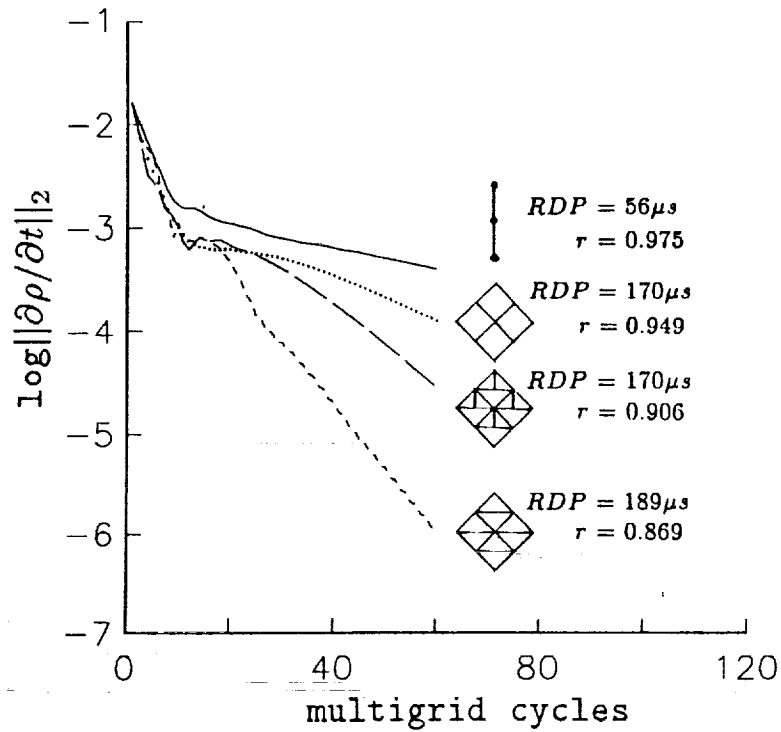
Figure **7**. Influence of multigrid strategies on convergence for ramp-flow problem.
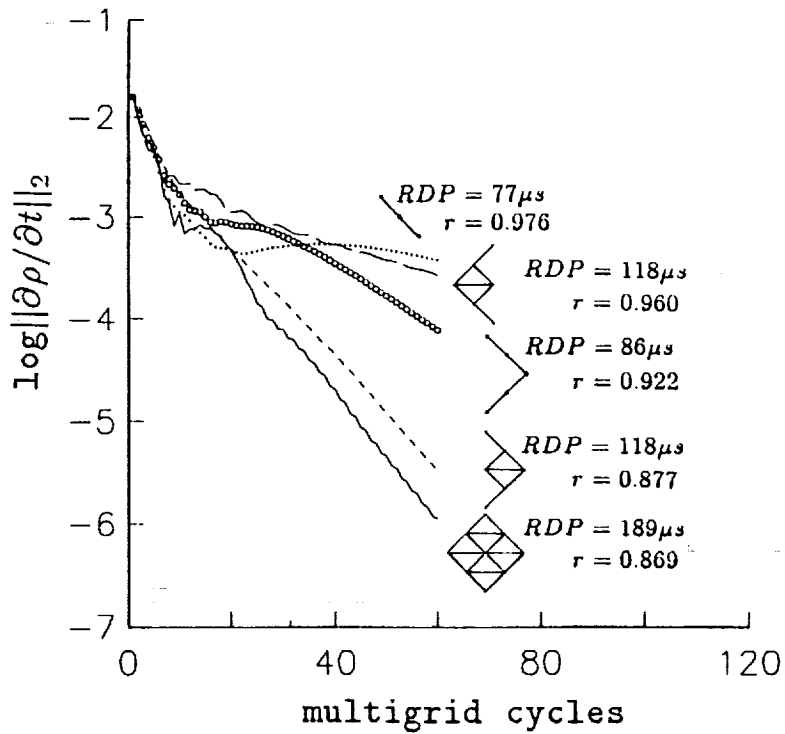
Figure **8**. Influence of selected coarse meshes on convergence for ramp-flow problem.

492
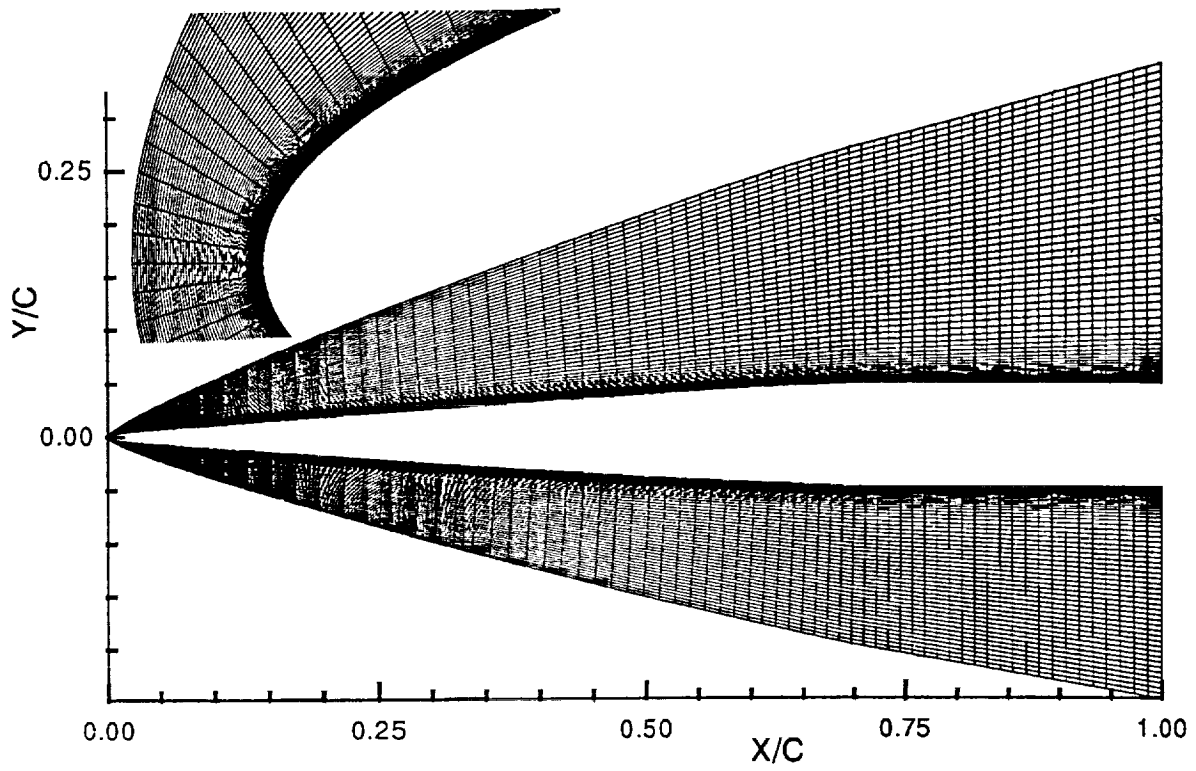
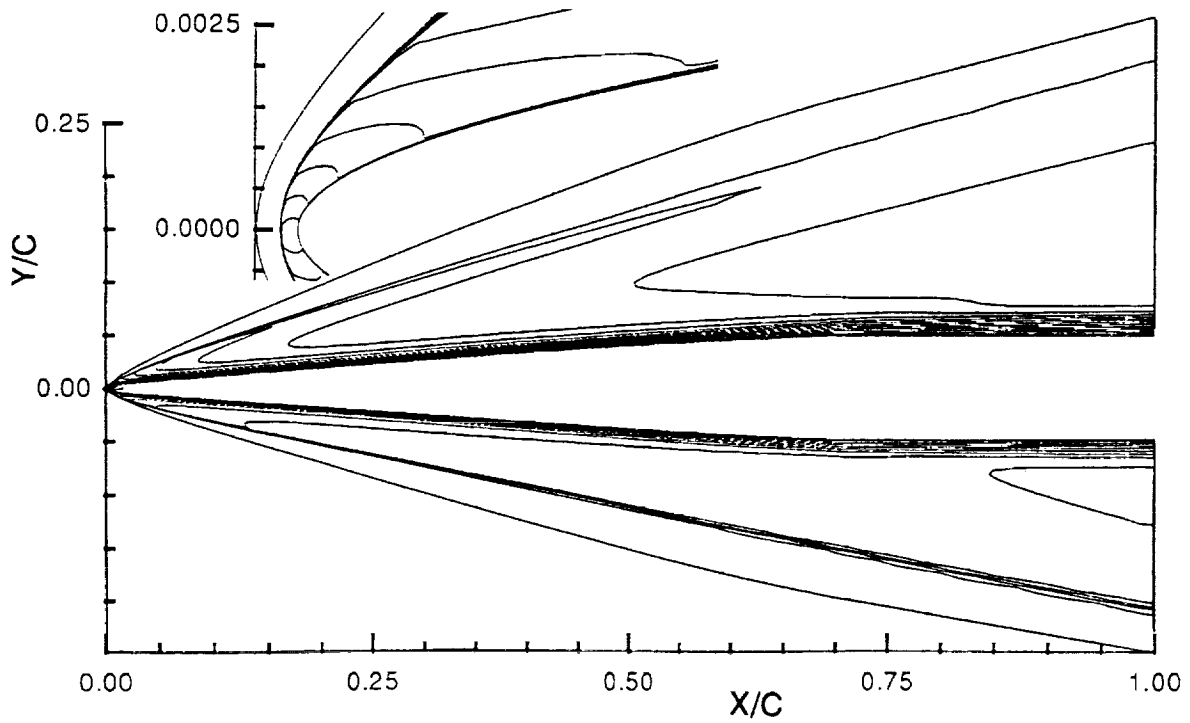Figure **9** . Coordinate mesh for forebody with 256x96 cells .
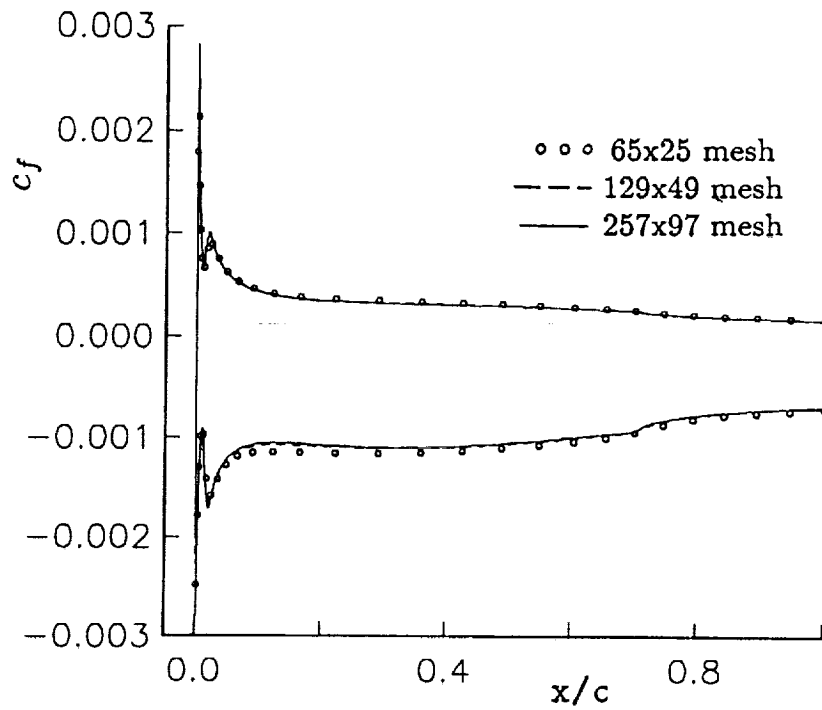

Figure **10**. Mach contours for turbulent forebody.

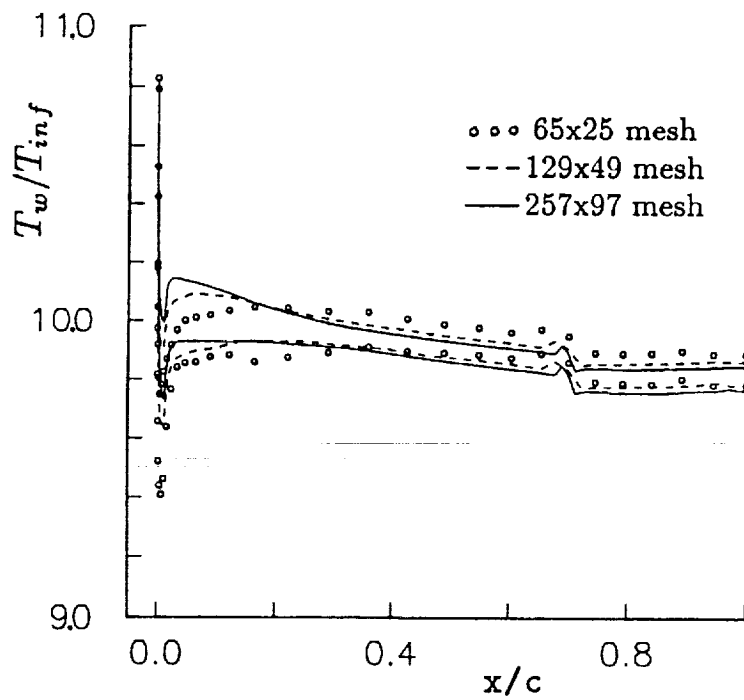Figure 11. Distribution of skin friction along forebody.

Figure 12. Distribution of adiabatic wall temperature along forebody.
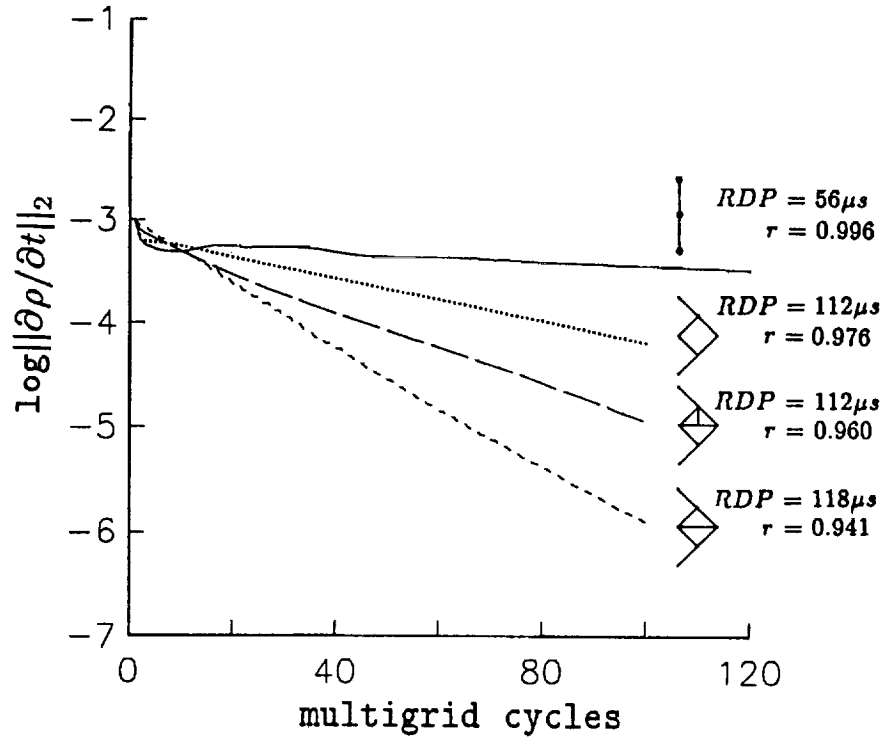
494

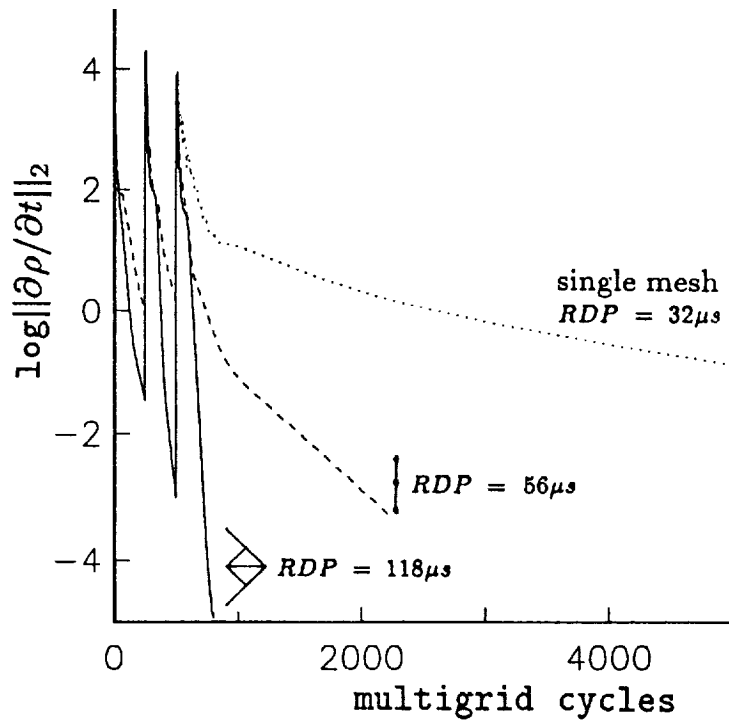Figure 13. Influence of multigrid strategy on convergence for forebody, mesh 256x96 .

Figure 14. Convergence histories for single-mesh time stepping and multigrid with sequential semicoarsening.